University of Plymouth

PEARL **https://pearl.plymouth.ac.uk**

Faculty of Science and Engineering School of Engineering, Computing and Mathematics

2021-11-15

Heat transfer modelling of carbon nanotube reinforced composites

Fang, Y

http://hdl.handle.net/10026.1/17761

10.1016/j.compositesb.2021.109280
Composites Part B: Engineering
Elsevier

All content in PEARL is protected by copyright law. Author manuscripts are made available in accordance with publisher policies. Please cite only the published version using the details provided on the item record or document. In the absence of an open licence (e.g. Creative Commons), permissions for further reuse of content should be sought from the publisher or author.

Published in "Composites Part B"
Received 14 June 2021/ Accepted 1 September 2021,
Available online 4 September 2021.
https://doi.org/10.1016/j.compositesb.2021.109280

Heat transfer modelling of carbon nanotube reinforced composites

Yuan Fang[1], Long-yuan Li[2*], Jean-Baptiste Mawulé Dassekpo[3], Sung-Hwan Jang[4]

1) Guangdong Provincial Key Laboratory of Durability for Maine Civil Engineering, Shenzhen University, Shenzhen 518060, P R China
2) School of Engineering, Computing and Mathematics, University of Plymouth, Plymouth, Devon PL4 8AA, UK (* Corresponding author)
3) Shenzhen Institute of Information Technology, Shenzhen 518172, P R China
4) School of Engineering, Hanyang University ERICA, Ansan, Gyeonggi-do 15588, South Korea

Abstract – In this paper an analytical prediction model for the heat transfer analysis of two-phase composite materials is developed. Formulations for the effective density, effective specific heat and effective thermal conductivity of the composite materials are derived. The present model considers not only the effect of interfacial thermal resistance between CNTs and polymer matrix but also the influence of fibre aspect ratio of CNTs on the effective thermal conductivity of the composites. The validation of the model is also provided by using available experimental data to demonstrate the appropriateness and reliability of the present model.

Keywords: Heat transfer; Thermal conductivity; Carbon nanotubes; Composites; Interfacial thermal resistance.

1. Introduction

Carbon nanotubes (CNTs) are cylindrical molecules, consisting of rolled-up sheets of single-layer carbon atoms. They can be single-walled with a diameter less than 1 nm or multi-walled with diameters larger than 100 nm. The latter usually consists of several concentrically interlinked nanotubes. The length of CNTs can reach several μm or even a few mm. CNTs have exceptional physical and mechanical properties and have been considered as the perfect building blocks in developing smart, multifunctional and high-performance composites.

Since they were discovered in early 1990s, CNTs have been used as the fillers or inclusions in matrix composites to improve the physical and mechanical properties of the composites. Typical examples include the functionally graded composites and smart sensors developed by means of CNTs' super mechanical and electrical properties. In recent decade, many researchers have attempted to use CNTs to improve the thermal properties of composites and studied the thermal performance of CNTs-reinforced composites. For instance, Zhang et al. [1] proposed a simplified approach for the heat transfer analysis of CNTs-based composites. In their model, the polymer was modelled as a domain, whereas the CNTs were treated as heat superconductors with constant and unknown temperatures constrained at their surfaces. Song and Youn [2] utilized the asymptotic expansion homogenization technique to evaluate the effective thermal conductivity (ETC) of polymeric composites filled with CNTs. Baniassadi et al. [3] reported a study on the ETC of polymer nanocomposites filled with CNTs using statistical continuum

theory. The predicted results were compared with experimental data in order to estimate the volume fraction of CNT agglomeration. Lizundia et al. [4] investigated experimentally the thermal properties of CNTs/poly(l-lactide) composites. The work demonstrated that the addition of CNTs could enhance the thermal conductivity of insulator polymers. Zhou et al. [5] presented a study on the thermal conductivity of flake graphite/polymer composites with carbon-based nano-fillers. It was shown that the thermal conductivity of the composites was increased by up to 24% and 31%, respectively when CNT and graphene was added at the level of 10wt.%. Hida et al. [6] reported the molecular dynamics study of heat conduction in CNTs/polyethylene composites. It was shown that there was a relatively high thermal boundary resistance across the CNTs/polyethylene interfaces, which affected the ETC of the composites. Huang et al. [7] investigated the thermal conductivity of epoxy matrix filled with poly (ethyleneimine) functionalized CNTs by using thermal gravimetric analysis, scanning electron microscope, and thermal analyser. It was shown that a 660% enhancement in thermal conductivity could be achieved when 8% PEI functionalized CNTs were added in the composite. Gardea and Lagoudas [8] investigated the thermal conductivity of epoxy composites with pristine, oxidized, and fluorinated CNTs. An increase of up to 5.5% was observed in thermal conductivity for the pristine CNTs composites, whereas the oxidized and fluorinated CNTs provided less enhancement. Gong et al. [9] developed a model by taking into account nano-filler orientation and morphology and interfacial thermal resistance between nano-fillers and polymer matrix. The model was used to predict the thermal conductivity of multiphase composite systems. Ahmed and Masud [10] presented a numerical simulation to evaluate the ETC of multi-walled CNTs-based polymer composites. The effects of CNTs diameter, length, volume fraction and thermal contact conductance on the ETC of CNTs-reinforced composites were examined. Kim et al. [11] investigated the thermal conductivity of cyclic butylene terephthalate-based composites containing CNTs and carbon blacks. Kundalwal et al. [12] reported a study on the ETC of fuzzy carbon fibre heat exchanger containing wavy CNTs. It was found that the fuzzy carbon fibre heat exchanger containing radially grown wavy CNTs has better heat transfer performance than that of the conventional hollow carbon fibre heat exchanger. Kuang and Huang [13] used the multi-scale approach, including large-scale molecular dynamics simulation, finite element simulation and analytical effective media modelling, to investigate the effects of covalent functionalization on the thermal transport in CNTs/polymer composites. Smith and Pantoya [14] examined the shape effect of nano-filler particles on the thermal energy transport in polytetrafluoroethylene matrix by using laser flash analysis method. TabkhPaz et al. [15] investigated the thermal conductivity of polymer composites filled with CNTs and hexagonal boron nitride by using 3-D random walk algorithm and effective medium approach. It was found that, for the composites with 13.1% of CNTs the increase in thermal conductivity was approximately 210%. However, for the hybrid composites with 3.1% of CNTs and hexagonal boron nitride (1.55% each), the increase in thermal conductivity was 290%. Ji et al. [16] provided a good review on the recent progress in the work related to thermal conduction of CNTs-reinforced polymer composites. The synthesis methods were also discussed along with the thermal property dependence on the aligned CNTs structure and morphology as well as the interface properties in the composites. Park et al. [17] presented an experimental study on the influence of different conditions of powder treatment on the thermal conductivity of nanocomposites, in which the thermal conductivity was determined by using laser flash method. Al-Ghalith et al. [18] investigated the influence of collapsed shape on the thermal transport of CNTs using molecular dynamics. CNTs of different lengths, diameters, chiralities, and degrees of twist were simulated in the regime where the thermal transport extends from ballistic to diffusive. Jensen et al. [19] presented a high strength material produced by directly bonding CNTs in high-strength sheets to introduce covalent linkages between the CNTs that affected their macroscale mechanical

properties. Choi et al. [20] examined the influence of interphase characteristics on the thermal conductivity of CNTs-reinforced polymer composites using a thermal resistance theory-based analytical model. Sung et al. [21] presented an analytical model to predict the thermal conductivity of multiscale hybrid composites, consisting of nano-fillers, micron-scale continuous fibres and polymer matrix. The method employed combines the modified Mori-Tanaka method and woven fibre composite modelling. The predicted thermal conductivity was validated using experimental results. Hassanzadeh-Aghdam et al. [22] investigated the effect of surface coating of CNTs on the ETC of unidirectional polymer hybrid nanocomposites. It was shown that the longitudinal ETC of CNTs-reinforced hybrid composites was not affected by the coating. However, the transverse ETC was significantly enhanced by the coating. Choi et al. [23] examined the effects of nitrogen-doped CNTs on the interphase characteristics of epoxy matrix nanocomposites by using molecular dynamics simulations. The results revealed that the interphase characteristics changed by the nitrogen-doped CNTs could significantly affect both the mechanical and thermal properties of the nanocomposites. Recently, Qi et al. [24] investigated the thermal conductivity of the poly(vinylidene fluoride) composites filled with boron nitride/CNTs. Yang et al. [25] experimentally examined the effects of the size, volume fraction and 3-D network organisation of CNTs on the thermal conductivity and thermal stability of CNTs-reinforced composites. More recently, good reviews were provided by Ruan et al. [26], Feng et al. [27], and Xu et al. [28] on the interfacial thermal resistance in thermally conductive polymer composites and the thermal properties, behaviour and performance of polymer-based composites.

The literature survey described above shows that there have been numerous experimental and numerical investigations but fewer prediction models on the thermal properties of CNTs-reinforced composites. Estimating thermal properties of composite materials, such as their effective specific heat and ETC, is essential for the understanding and controlling of thermal transport taking place in CNTs-reinforced composite materials. The existing prediction models for thermal conductivity can be categorised into three groups. The first one was directly to use Maxwell model for spherical inclusions or Halpin-Tsai model for non-spherical inclusions, for example, [29]. This kind of models considered the effect of aspect ratio of inclusions but not the interfacial thermal resistance. The second one was the modified version of Halpin-Tsai model in which the interfacial thermal resistance was deployed in the model by first modifying the thermal conductivity of inclusions [30,31,32]. However, the use of recursive formulas in Halpin-Tsai model is difficult to verify mathematically and thus the model is only semi-empirical. The third one was derived mathematically based on the concept of Maxwell model but also considered the interfacial thermal resistance between inclusions and matrix [33,34]. However, this kind of models are only applicable to the composites with spherical inclusions. In this paper, an analytical model is proposed to predict the thermal properties of CNTs-reinforced composites. The model is developed based on the concept of Maxwell model but considers the effects of both the interfacial thermal resistance and aspect ratio of inclusions. Compared to existing models, the present model has the following features. Firstly, the ETC is derived exactly based on the solutions of heat transfer in two-phase composites; secondly, the model also provides the upper- and lower-bounds of ETC; thirdly, the ETC derived considers not only the effect of interfacial thermal resistance, but also the influences of aspect ratio and percolation threshold of inclusions; fourthly, the model is validated using the experimental data published in literature in order to demonstrate its appropriateness and reliability.

2. Description of heat transfer analysis in two-phase composites

Consider a two-phase composite material, in which one is the homogeneous medium and the other represents a finite number of inclusions. The governing equation for the heat transfer analysis of the composite is well known and can be expressed as follows,

$$(\rho_i c_i)\frac{\partial T_i}{\partial t} = \nabla(k_i \nabla T_i) \qquad \text{in } \Omega_i \ \ (\text{i=1,2}) \qquad (1)$$

where ρ_i is the density, c_i is the specific heat, T_i is the temperature, t is the time, k_i is the thermal conductivity, the subscript i refers to component i in the composite, and Ω_i is the domain of component i (i=1 for the inclusions and i=2 for the medium matrix). For a multi-phase composite additional equations are required to define the temperature and heat flux at the interfaces between different components. For the two-phase composite, these can be expressed as follows,

$$k_i \nabla T_i = h(T_2 - T_1) \qquad \text{on } \Gamma_{12} \ (\text{i=1,2}) \qquad (2)$$

where h is the "convective" coefficient reflecting the thermal resistance at the interface when the heat is transferred from one component to another [33], and Γ_{12} is the interface between component 1 and component 2. If the interfacial thermal resistance is dominated by radiation, h should be temperature-dependent [34]. It is obvious by observing Eq.(2) that, $h \to \infty$ means that there is no interfacial thermal resistance and thus Eq.(2) reduces to $T_1=T_2$ and $k_1 \nabla T_1 = k_2 \nabla T_2$, that is the conventional continuous conditions for temperature and heat flux; whereas $h \to 0$ means that there is no heat transfer taking place at the interface and in this case all of the inclusions embedded in the medium are thermally isolated.

Interfacial thermal resistance is a measure of an interface's resistance to thermal flow. It arises at the boundary between two different phase materials owing to their differences in electronic and vibrational properties. When an energy carrier attempts to traverse the interface, it will scatter at the interface. The probability of the transmission after scattering will depend on the available energy states on the two sides of the interface. The type of carrier scattered will also depend on the materials governing the interfaces. Hence, in general, the interfacial thermal resistance should depend on the properties of the materials on the two sides of the interface. Understanding the thermal resistance at the interface between two distinct materials is of primary significance in the study of its thermal properties. Interfaces often contribute significantly to the observed properties of the materials [35], but the exact mechanism of the resistance is not fully understood [36,37,38,39].

In principle, the governing equations (1) and (2) together with initial and boundary conditions can be solved using various numerical methods, for instance, [1]. However, practically, to execute such numerical simulations is rather difficult for a macro-scale structure because the CNTs-reinforced composite often involves massive number of small size CNTs. To overcome the computational problem efforts have been made to develop mesoscopic analysis model to determine the effective thermal properties of the composite [33,34,40]. If the effective thermal properties of a composite can be appropriately determined, then the heat transfer analysis of the two-phase composite material can be treated as a normal single-phase material. The effective thermal properties of a two-phase composite are dependent not only on the thermal properties and volume fractions of the two constituted materials but also on the manner how the two components are mixed and organised in the composite. In the present study, we follow the approach outlined in [40,41] by treating the composite, consisting of spherical inclusions, but with modifications by taking into account the effects of interfacial thermal resistance, aspect

ratio and percolation of the inclusions. The latter is particularly important for the CNTs-reinforced polymer composites.

3. Effective thermal properties of two-phase composite materials

Fig.1a shows the representative volume element (RVE) of a two-phase composite used in the spherical model, in which the inner sphere represents the volume of inclusions and the outer shell stands for the volume of medium. The volume fractions of the inclusions and medium in the RVE thus can be expressed as follows,

$$V_1 = \left(\frac{R_1}{R_2}\right)^3 \tag{3}$$

$$V_2 = 1 - \left(\frac{R_1}{R_2}\right)^3 \tag{4}$$

where V_1 and V_2 are the volume fractions of the inclusions and medium, respectively, R_1 is the radius of the inner sphere, and R_2 is the outer radius of the shell (see Fig.1a). Assume that the interface between the inclusion and medium does not absorb thermal energy. Then, the effective density and effective specific heat of the composite material can be calculated as follows,

$$\rho_e = \rho_1 V_1 + \rho_2 V_2 \tag{5}$$

$$c_e = \frac{c_1\rho_1 V_1 + c_2\rho_2 V_2}{\rho_1 V_1 + \rho_2 V_2} \tag{6}$$

where ρ_e and c_e are the effective density and effective specific heat of the composite material, ρ_1 and c_1 are the density and specific heat of the inclusion material, ρ_2 and c_2 are the density and specific heat of the medium material, respectively.

The ETC of the two-phase composite material can be derived by using the concept of equivalence between a single-phase material and a two-phase composite material in terms of the temperature and heat flux. By using the spherical model (Fig.1a) the heat transfer equation at steady state can be expressed as follows,

$$\frac{1}{r^2}\frac{\partial}{\partial r}\left(k_i r^2 \frac{\partial T_i}{\partial r}\right) + \frac{1}{r^2 \sin\theta}\frac{\partial}{\partial \theta}\left(k_i \sin\theta \frac{\partial T_i}{\partial \theta}\right) = 0 \qquad \text{in } \Omega_i \quad (i=1,2) \tag{7}$$

where (r,θ,φ) are the spherical coordinates with the coordinate origin imposed at the common centre of the spheres, Ω_1 is the domain of $r<R_1$, and Ω_2 is the domain of $R_1<r<R_2$. The axial symmetry is assumed to be around x_3-axis where $x_3=r\cos\theta$. The boundary condition of the temperature or heat flux is defined at its infinity ($x_3\to\infty$). The general solution of Eq.(7) can be expressed as follows,

$$T_i(r,\theta,\varphi) = \left(A_i r + \frac{B_i}{r^2}\right)\cos\theta \qquad \text{in } \Omega_i \quad (i=1,2) \tag{8}$$

where A_i and B_i (i=1,2) are the constants to be determined. Note that constant B_1 must vanish due to the singularity at the origin. Constant A_2 can be determined based on the imposed remote boundary condition. Constants A_1 and B_2 are determined according to the thermal resistance at the interface ($r=R_1$), which, according to Eq.(2), can be expressed as follows,

$$k_1 \frac{\partial T_1}{\partial r}\Big|_{r=R_1} = k_2 \frac{\partial T_2}{\partial r}\Big|_{r=R_1} \tag{9}$$

$$k_1 \frac{\partial T_1}{\partial r}\Big|_{r=R_1} = h(T_2 - T_1)|_{r=R_1} \tag{10}$$

Substituting Eq.(8) into Eqs.(9) and (10), the following expressions for A_1 and B_2 are obtained,

$$A_1 = \frac{3A_2}{\left(2+\frac{2k_1}{hR_1}+\frac{k_1}{k_2}\right)} \tag{11}$$

$$\frac{B_2}{R_1^3} = \frac{\left(1+\frac{k_1}{hR_1}-\frac{k_1}{k_2}\right)A_2}{\left(2+\frac{2k_1}{hR_1}+\frac{k_1}{k_2}\right)} \tag{12}$$

It can be observed that, when $h\to\infty$ Eqs.(11) and (12) give the same formulations as those derived in the Maxwell model [34]; and when $h\to 0$ Eqs.(11) and (12) lead to $A_1\to 0$ and $B_2\to R_1^3 A_2/2$, indicating that the heat transfer happens only in the medium.

We now consider the RVE of a single material of the same size as shown in Fig.1a. The solution of Eq.(7) in the RVE ($\Omega = \Omega_1 + \Omega_2$) can be expressed as follows,

$$T_e(r,\theta,\varphi) = \left(A_e r + \frac{B_e}{r^2}\right)\cos\theta \qquad \text{in } \Omega \tag{13}$$

where T_e is the temperature, A_e and B_e are the constants to be determined. The following two equations must be satisfied if the single material model is equivalent to the two-phase composite material in terms of the temperature and heat flux at the outside edge of the sphere,

$$T_e|_{r=R_2} = T_2|_{r=R_2} \tag{14}$$

$$k_e \frac{\partial T_e}{\partial r}\Big|_{r=R_2} = k_2 \frac{\partial T_2}{\partial r}\Big|_{r=R_2} \tag{15}$$

where k_e is the ETC. Substituting Eqs.(8) and (13) into (14) and (15) and noting that constant B_e must be zero due to the singularity at the origin, it yields,

$$k_{e,min} = k_e = k_2 \frac{\left(2+\frac{2k_1}{hR_1}+\frac{k_1}{k_2}\right)-2V_1\left(1+\frac{k_1}{hR_1}-\frac{k_1}{k_2}\right)}{\left(2+\frac{2k_1}{hR_1}+\frac{k_1}{k_2}\right)+V_1\left(1+\frac{k_1}{hR_1}-\frac{k_1}{k_2}\right)} \tag{16}$$

Eq.(16) gives the ETC of the two-phase composite material. Since the model assumes all inclusions, which have higher thermal conductivity, are perfectly embedded in the medium, which has lower thermal conductivity, k_e predicted by Eq.(16) represents the lower-bound of ETC, and thus it is designated as $k_{e,min}$.

For the case of $h\to\infty$ where there is no interfacial thermal resistance Eq.(16) reduces to the Maxwell model [34,40]; whereas for $h\to 0$ where all inclusions are completely isolated Eq.(16) reduces to the Maxwell model with $k_1=0$ [34,40]. As an example, Fig.2 plots the variation of the lower-bound ETC with the volume fraction of inclusions for different interfacial thermal resistances. It can be seen from the figure that, for the cases of $hR_1=\infty$ and $hR_1=k_1$ the lower-bound ETC increases with the volume fraction of inclusions, but for the case of $hR_1=k_2$ it

decreases slightly with the increased volume fraction of inclusions. The latter is because the high thermal conductivity in inclusions is overtaken by the high interfacial thermal resistance on the inclusions' surfaces. Also, it can be seen from the figure that, if the interfacial thermal resistance is similar to the inclusions' conductivity, the lower-bound ETC reduces almost by a half when the volume fraction of inclusions tends to 1.

In general, Eq.(16) is only suitable to the composite with no percolated inclusions or with very low volume fraction of inclusions. The percolation threshold of CNTs-reinforced composite is very low because of the large aspect ratio of CNTs fibres [41,42]. To take account for the effects of aspect ratio and percolation threshold of CNTs on the ETC, we also need know the upper-bound of the ETC. By assuming all inclusions are fully percolated, the positions of the inclusions and medium in the spherical model shown in Fig.1a need be swapped, that is, the inner sphere is to represent the volume of medium, whereas the outer shell is to stand for the volume of inclusions. The swapped volumes in the spherical model is shown in Fig.1b. In this case, the upper-bound of the ETC of the two-phase composite material can be obtained from Eq.(16) by swapping $k_1 \leftrightarrow k_2$ and $V_1 \leftrightarrow (1-V_1)$, that is,

$$k_{e,max} = k_e = k_1 \frac{\left(2+\frac{2k_2}{hR_1}+\frac{k_2}{k_1}\right)-2(1-V_1)\left(1+\frac{k_2}{hR_1}-\frac{k_2}{k_1}\right)}{\left(2+\frac{2k_2}{hR_1}+\frac{k_2}{k_1}\right)+(1-V_1)\left(1+\frac{k_2}{hR_1}-\frac{k_2}{k_1}\right)} \tag{17}$$

where $k_{e,max}$ is the upper-bound ETC of the two-phase composite material. Fig.3 plots the variation of the upper-bound ETC with the volume fraction of inclusions for different interfacial thermal resistances. It can be seen from the figure that the upper-bound ETC increases with increased volume fraction of inclusions. There is a little difference in $k_{e,max}$ between the cases of $hR_1=\infty$ and $hR_1=k_1$. The $k_{e,max}$ for the case of $hR_1=k_2$ is only slightly smaller than that of $hR_1=\infty$, indicating that the influence of the interfacial thermal resistance on the upper-bound ETC is not significant.

Eqs.(16) and (17) represent the two extreme cases of the inclusions mixed in the two-phase composite. In real cases, however, neither the medium nor the inclusion would be perfectly covered by the medium or by the inclusion. To consider the random distribution and random dispersion of inclusions in the composite, we herein consider a unit volume of RVE (Fig.4). Assume that the inclusions in the RVE are equally spread in x-, y-, and z-axial directions and can be approximately characterised by the configuration of three-prisms with dimensions [λa, a, a] as shown in Fig.4, where λ is the aspect ratio of inclusions and a is a virtual length parameter. For simplicity, the shape of inclusions is assumed to like solid fibres and the cross-section effect of inclusions is ignored. For a given λ, the virtual length, a, can be calculated based on the volume fraction of inclusions in the composite according to Eq.(18) or Eq.(21) [41]. According to the configuration shown in Fig.4a, we have.

If $\lambda a < 1$,

$$V_1 = 3\lambda a^3 - 2a^3 = (3\lambda - 2)a^3 \tag{18}$$

$$V_{m1} = (\lambda a)^3 - (3\lambda-2)a^3 = (\lambda^3 - 3\lambda+2)a^3 \tag{19}$$

$$V_{m2} = 1 - (\lambda a)^3 \tag{20}$$

If $\lambda a = 1$,

$$V_1 = 3\lambda a^3 - 2a^3 = (3-2a)a^2 \tag{21}$$

$$V_{m1} = 1 - (3-2a)a^2 \tag{22}$$

$$V_{m2} = 0 \tag{23}$$

where V_{m1} is the volume of the medium in the sub-domain shown in Fig.4b, V_{m2} is the volume of the medium in the unit volume of the cube subtract the sub-domain, and $V_{m1}+V_{m2}=V_2$ is the volume fraction of the medium in the composite.

The ETC of the RVE can be calculated by two steps [41]. The first step is to calculate the ETC of the sub-domain shown in Fig.4b by using Eq.(17), in which the medium (V_{1m}) is completely covered by the inclusions (V_1) or the inclusions are fully percolated,

$$k_e^1 = k_1 \frac{\left(2+\frac{2k_2}{hR_1}+\frac{k_2}{k_1}\right)-2\left(1-\frac{V_1}{V_1+V_{m1}}\right)\left(1+\frac{k_2}{hR_1}-\frac{k_2}{k_1}\right)}{\left(2+\frac{2k_2}{hR_1}+\frac{k_2}{k_1}\right)+\left(1-\frac{V_1}{V_1+V_{m1}}\right)\left(1+\frac{k_2}{hR_1}-\frac{k_2}{k_1}\right)} \tag{24}$$

where k_e^1 is the ETC of the sub-domain. The second step is to calculate the ETC of the RVE shown in Fig.4a by using Eq.(16), in which the sub-domain (V_1+V_{1m}) with ETC k_e^1 is completely covered by the medium (V_{2m}) or the sub-domain is not percolated in the RVE,

$$k_{eff} = k_2 \frac{\left(2+\frac{2k_e^1}{hR_1}+\frac{k_e^1}{k_2}\right)-2(V_1+V_{m1})\left(1+\frac{k_e^1}{hR_1}-\frac{k_e^1}{k_2}\right)}{\left(2+\frac{2k_e^1}{hR_1}+\frac{k_e^1}{k_2}\right)+(V_1+V_{m1})\left(1+\frac{k_e^1}{hR_1}-\frac{k_e^1}{k_2}\right)} \tag{25}$$

where k_{eff} is the ETC of the RVE. Eq.(25) provides a general formulation for calculating the ETC of two-phase composite materials. For a given composite, one can first calculate V_{1m} and V_{2m} using Eqs.(19) and (20) or Eqs.(22) and (23) based on λ and V_1, followed by using Eqs.(24) and (25) to calculate k_e^1 and k_{eff}. Since the volume fraction (V_{m1}) of the medium in the sub-domain is dependent on not only the volume fraction but also the aspect ratio of inclusions, the ETC calculated using Eq.(25) not only includes the effect of the interfacial thermal resistance but also the effect from the aspect ratio and percolation of inclusions; the latter has been discussed in the calculation of the effective electrical conductivity of composites [41,43,44,45,46]. Fig.5 graphically shows the difference between the k_{eff} calculated using Eq.(25) and the $k_{e,min}$ and $k_{e,max}$ calculated using Eqs.(16) and (17). It can be seen from the figure that, unlike $k_{e,min}$ and $k_{e,max}$, k_{eff} is able to reflect the effect of aspect ratio of inclusions on the ETC. It is closer to $k_{e,min}$ when the volume fraction of inclusions is very small and to $k_{e,max}$ when the volume fraction of inclusions becomes large. When the interfacial thermal resistance is not considered the transition of k_{eff} from $k_{e,min}$ to $k_{e,max}$ is rather smooth. However, when the interfacial thermal resistance is considered there is a jump in k_{eff} happened at the percolation threshold of inclusions. The larger the aspect ratio of inclusions, the smaller the percolation threshold of inclusions. Comparing Fig.5a and Fig.5b, one can see the ETC is smaller when the interfacial thermal resistance is considered until the volume fraction of inclusions reaches to its threshold value.

4. Simplified model applied to CNTs-reinforced two-phase composite materials

For most CNTs-reinforced two-phase composite materials the thermal conductivity of CNTs is much higher than that of the medium material and the volume fraction of CNTs is much small in the composite. In this case, Eqs.(24) can be simplified as follows owing to the fact of $k_1 >> k_2$,

$$\frac{k_e^1}{k_1} \approx \frac{\left(2+\frac{2k_2}{hR_1}\right)-2\left(1-\frac{V_1}{V_1+V_{m1}}\right)\left(1+\frac{k_2}{hR_1}\right)}{\left(2+\frac{2k_2}{hR_1}\right)+\left(1-\frac{V_1}{V_1+V_{m1}}\right)\left(1+\frac{k_2}{hR_1}\right)} = \frac{\frac{2V_1}{V_1+V_{m1}}}{3-\frac{V_1}{V_1+V_{m1}}} = \frac{2V_1}{2V_1+3V_{m1}} \tag{26}$$

Eq.(26) indicates that k_e^1 is in the similar order of magnitude of k_1. Similarly, Eq.(25) can be simplified as follows owing to the fact of $k_e^1 \gg k_2$,

$$\frac{k_{eff}}{k_2} \approx \frac{\left(\frac{2k_2}{hR_1}+1\right)-2(V_1+V_{m1})\left(\frac{k_2}{hR_1}-1\right)}{\left(\frac{2k_2}{hR_1}+1\right)+(V_1+V_{m1})\left(\frac{k_2}{hR_1}-1\right)} \tag{27}$$

Eqs.(26) and (27) can be used to calculate the ETC of CNTs-reinforced composites with and without percolated CNTs, respectively. It is of interest to notice that, for a CNTs-percolated composite ($V_{m2}=0$) its ETC is linearly proportional to the thermal conductivity of CNTs material (see Eq.(26)); whereas for a composite in which CNTs are not percolated ($V_{m2}>0$), its ETC is linearly proportional to the thermal conductivity of medium material (see Eq.(27)). The proportional factor depends on the volume fraction of inclusions in the former and the interfacial thermal resistance and volume fraction and percolation threshold of inclusions in the latter.

To validate the present model, experimental data are used for three different composite materials. The first set of the experimental data is for the composite made from epoxy filled with aluminium nitride (AlN) particles of sizes 90-100 μm [47]. In the experiments seven different volume fractions of AlN particles ranging from 0 to 15% were used and the corresponding ETCs of the composites were measured [47]. The comparison between the measured ETC and predicted ETC using Eq.(27) is shown in Fig.6. In the calculation the thermal conductivity of the epoxy and AlN was taken as k_2=0.363 W/(m·K) and k_1=160 W/(m·K), respectively, which were obtained from the experiments [47]. The aspect ratio of AlN particles and interfacial thermal resistance used in the calculation were assumed as λ=2.65 and $hR_1=5k_2$, which were obtained by best matching the experimental data. It can be seen from the figure that the predicted ETC is in good agreement with the measured ETC.

The second set of experimental data is the CNTs-reinforced poly (l-lactide) (PLLA) composite. In the experiments six different volume fractions of CNTs ranging from 0 to 3.04% were used and the corresponding thermal diffusivities of the composites were measured [48]. The experimental ETCs were calculated based on the measured thermal diffusivity, effective density, and effective specific heat. The comparison between the experimental ETC and predicted ETC using Eq.(27) is shown in Fig.7. In the calculation the thermal conductivity of the PLLA and CNTs was taken as k_2=0.10 W/(m·K) and k_1=750 W/(m·K), respectively, which were obtained from the experiments [48]. The aspect ratio of CNTs fibres and interfacial thermal resistance used in the calculation were assumed as λ=8 and $hR_1=5k_2$, which were obtained by best matching the experimental data. It can be seen from the comparison shown in Fig.7 that the predicted ETC agrees very well with the experimentally obtained ETC.

The third set of experimental data is the single-walled CNTs-reinforced poly (methyl methacrylate) (PMMA) composite. In the experiments CNTs were prepared through floating catalyst chemical vapour deposition method and were dispersed uniformly in PMMA matrix

[49,50]. Five different mass fractions of CNTs ranging from 0 to 4.0% were used and their corresponding ETCs were measured. The mass fraction of CNTs is converted to the volume fraction of CNTs by using the following equation,

$$V_1 = \frac{m_1\rho_2}{m_1\rho_2-(1-m_1)\rho_1} \tag{28}$$

where ρ_1=2250 kg/m^3 and ρ_2=1180 kg/m^3 are the densities of the CNTs and hardened PMMA materials, respectively, m_1 is the mass fraction of CNTs in the composite. The comparison between the measured ETC and predicted ETC using Eq.(27) is also shown in Fig.7. In the calculation the thermal conductivity of the PMMA and CNTs was taken as k_2=0.45 W/(m·K) and k_1=750 W/(m·K), respectively, which were obtained from the experiments [50]. The aspect ratio of CNTs fibres and interfacial thermal resistance used in the calculation were assumed as λ=8 and $hR_1=5k_2$, which were obtained by best matching the experimental data. Again, a good agreement between the predicted and measured ETCs is demonstrated.

5. Conclusions

This paper has presented an analytical model for calculating the ETC of two-phase composite materials. The model has been validated by using experimental data published in literature. From the results obtained we have the following conclusions.

- For CNTs-reinforced composites where the thermal conductivity of CNTs is much greater than that of the medium material, the ETC of the composite material is linearly proportional to that of the medium material if the CNTs are not percolated in the composite (see Eq.(27)). However, if the CNTs are fully percolated in the composite then the ETC of the composite material is linearly proportional to that of the CNTs (see Eq.(26)). This is agreed with what was observed in experiments [51,52,53].

- The interfacial thermal resistance has important influence on the ETC of the composite material but only for the case where the CNTs are not fully percolated. The higher the interfacial thermal resistance, the lower the ETC of the composite material. For the composite where CNTs are fully percolated, the influence of interfacial thermal resistance on the ETC is very small and could be ignored.

- The aspect ratio of CNTs has dominant influence on the ETC of CNTs-reinforced composite materials. However, the threshold volume fraction of CNTs for ETC seems much larger than that for effective electrical conductivity for the same composite because of the influence of interfacial thermal resistance. The higher threshold volume fraction of CNTs limits the heat transfer in the composite and thus leads to low ETC.

Acknowledgments – The work presented in the paper was supported by the National Natural Science Foundation of China (grant No. 52078300) and the Ministry of Land, Infrastructure and Transport of South Korea (grant No. 21CTAP-C151808-03).

Declaration of interests - The authors declare that they have no known competing financial interests or personal relationships that could have appeared to influence the work reported in this paper.

References

[1] J. Zhang, M. Tanaka, T. Matsumoto, A simplified approach for heat conduction analysis of CNT-based nano-composites, Computer Methods in Applied Mechanics and Engineering 193(52) (2004) 5597-5609.

[2] Y.S. Song, J.R. Youn, Evaluation of effective thermal conductivity for carbon nanotube/polymer composites using control volume finite element method, Carbon 44(4) (2006) 710-717.

[3] M. Baniassadi, A. Laachachi, A. Makradi, S. Belouettar, D. Ruch, R. Muller, H. Garmestani, V. Toniazzo, S. Ahzi, Statistical continuum theory for the effective conductivity of carbon nanotubes filled polymer composites, Thermochimica Acta 520(1–2) (2011) 33-37.

[4] E. Lizundia, A. Oleaga, A. Salazar, J.R. Sarasua, Nano- and microstructural effects on thermal properties of poly (l-lactide)/multi-wall carbon nanotube composites, Polymer 53(12) (2012) 2412-2421.

[5] S. Zhou, J. Xu, Q.-H. Yang, S. Chiang, B. Li, H. Du, C. Xu, F. Kang, Experiments and modeling of thermal conductivity of flake graphite/polymer composites affected by adding carbon-based nano-fillers, Carbon 57 (2013) 452-459.

[6] S. Hida, T. Hori, T. Shiga, J. Elliott, J. Shiomi, Thermal resistance and phonon scattering at the interface between carbon nanotube and amorphous polyethylene, International Journal of Heat and Mass Transfer 67 (2013) 1024-1029.

[7] J. Huang, M. Gao, T. Pan, Y. Zhang, Y. Lin, Effective thermal conductivity of epoxy matrix filled with poly(ethyleneimine) functionalized carbon nanotubes, Composites Science and Technology 95 (2014) 16-20.

[8] F. Gardea, D.C. Lagoudas, Characterization of electrical and thermal properties of carbon nanotube/epoxy composites, Composites Part B: Engineering 56 (2014) 611-620.

[9] F. Gong, K. Bui, D.V. Papavassiliou, H.M. Duong, Thermal transport phenomena and limitations in heterogeneous polymer composites containing carbon nanotubes and inorganic nanoparticles, Carbon 78 (2014) 305-316.

[10] S. Ahmed, A.K.M. Masud, Evaluation of effective thermal conductivity of multiwalled carbon nanotube reinforced polymer composites using finite element method and continuum model, Procedia Engineering 90 (2014) 129-135.

[11] S.Y. Kim, Y.J. Noh, J. Yu, Improved thermal conductivity of polymeric composites fabricated by solvent-free processing for the enhanced dispersion of nanofillers and a theoretical approach for composites containing multiple heterogeneities and geometrized nanofillers, Composites Science and Technology 101 (2014) 79-85.

[12] S.I. Kundalwal, R.S. Kumar, M.C. Ray, Effective thermal conductivities of a novel fuzzy carbon fiber heat exchanger containing wavy carbon nanotubes, International Journal of Heat and Mass Transfer 72 (2014) 440-451.

[13] Y. Kuang, B. Huang, Effects of covalent functionalization on the thermal transport in carbon nanotube/polymer composites: A multi-scale investigation, Polymer 56 (2015) 563-571.

[14] D.K. Smith, M.L. Pantoya, Effect of nanofiller shape on effective thermal conductivity of fluoropolymer composites, Composites Science and Technology 118 (2015) 251-256.

[15] M. TabkhPaz., S. Shajari, M. Mahmoodi, D.-Y. Park, H. Suresh, S.S. Park, Thermal conductivity of carbon nanotube and hexagonal boron nitride polymer composites, Composites Part B: Engineering 100 (2016) 19-30.

[16] T. Ji, Y. Feng, M. Qin, W. Feng, Thermal conducting properties of aligned carbon nanotubes and their polymer composites, Composites Part A: Applied Science and Manufacturing 91 (2016) 351-369.

[17] H.J. Park, A. Badakhsh, I.T. Im, M.-S. Kim, C.W. Park, Experimental study on the thermal and mechanical properties of MWCNT/polymer and Cu/polymer composites, Applied Thermal Engineering 107 (2016) 907-917.
[18] J. Al-Ghalith, H. Xu, T. Dumitrică, Collapsed carbon nanotubes as building blocks for high-performance thermal materials, Physical Review Materials 1(5) (2017) 056001.
[19] B.D. Jensen, J.W. Kim, G. Sauti, K.E. Wise, L. Dong, H.N.G. Wadley, J.G. Park, R. Liang, E.J. Siochi, Toward ultralight high-strength structural materials via collapsed carbon nanotube bonding, Carbon 156 (2020) 538-548.
[20] H.K. Choi, H. Jung, Y. Oh, H. Hong, J. Yu, E.S. Shin, Analysis of the influence of interphase characteristics on thermal conduction in surface-modified carbon nanotube-reinforced composites using an analytical model, Composites Science and Technology 168 (2018) 145-151.
[21] D.H. Sung, M. Kim, Y.-B. Park, Prediction of thermal conductivities of carbon-containing fiber-reinforced and multiscale hybrid composites, Composites Part B: Engineering 133 (2018) 232-239.
[22] M.K. Hassanzadeh-Aghdam, M.J. Mahmoodi, J. Jamali, Effect of CNT coating on the overall thermal conductivity of unidirectional polymer hybrid nanocomposites, International Journal of Heat and Mass Transfer 124 (2018) 190-200.
[23] H.K. Choi, H. Jung, Y. Oh, H. Hong, J. Yu, E.S. Shin, Interfacial effects of nitrogen-doped carbon nanotubes on mechanical and thermal properties of nanocomposites: A molecular dynamics study, Composites Part B: Engineering 167 (2019) 615-620.
[24] X.-D. Qi, W.-Y. Wang, Y.-J. Xiao, T. Huang, N. Zhang, J.-H. Yang, Y. Wang, Tailoring the hybrid network structure of boron nitride/carbon nanotube to achieve thermally conductive poly(vinylidene fluoride) composites, Composites Communications 13 (2019) 30-36.
[25] W. Yang, J. Xiong, L. Wu, Y. Du, Methods for enhancing the thermal properties of epoxy matrix composites using 3D network structures, Composites Communications 12 (2019) 14-20.
[26] K. Ruan, X. Shi, Y. Guo, J. Gu, Interfacial thermal resistance in thermally conductive polymer composites: A review, Composites Communications 22 (2020) 100518.
[27] C.-P. Feng, L.-Y. Yang, J. Yang, L. Bai, R.-Y. Bao, Z.-Y. Liu, M.-B. Yang, H.-B. Lan, W. Yang, Recent advances in polymer-based thermal interface materials for thermal management: A mini-review, Composites Communications 22 (2020) 100528.
[28] Y. Xu, X. Wang, Q. Hao, A mini review on thermally conductive polymers and polymer-based composites, Composites Communications 24 (2021) 100617.
[29] C.W. Nan, Z. Shi, Y. Lin, A simple model for thermal conductivity of carbon nanotube-based composites, Chemical Physics Letters 375(5-6) (2003) 666-669.
[30] C.W. Nan, R. Birringer, D.R. Clarke, H. Gleiter, Effective thermal conductivity of particulate composites with interfacial thermal resistance, Journal of Applied Physics 81(10) (1997) 6692–6699.
[31] M.K. Hassanzadeh-Aghdam, M.J. Mahmoodi, J. Jamali, R. Ansari, A new micromechanical method for the analysis of thermal conductivities of unidirectional fiber/CNT-reinforced polymer hybrid nanocomposites, Composites Part B: Engineering 175 (2019) 107137.
[32] M. Safi, M.K. Hassanzadeh-Aghdam, M.J. Mahmoodi, A semi-empirical model for thermal conductivity of polymer nanocomposites containing carbon nanotubes, Polymer Bulletin volume 77(12) (2020) 6577–6590.
[33] D.P.H. Hasselman, L.F. Johnson, Effective thermal conductivity of composites with interfacial thermal barrier resistance, Journal of Composite Materials 21 (1987) 508-515.

[34] K.B. Kiradjiev, S.A. Halvorsen, R.A. Van Gorder, S.D. Howison, Maxwell-type models for the effective thermal conductivity of a porous material with radiative transfer in the voids, International Journal of Thermal Sciences 145 (2019) 106009.
[35] M. Li, J. Kang, H. Nguyen, H. Wu, Y. Hu, Anisotropic thermal boundary resistance across 2D black phosphorus: experiment and atomistic modeling of interfacial energy transport, Advanced Materials 31(33) (2019) 1901021.
[36] H.L. Zhong, J.R. Lukes, Interfacial thermal resistance between carbon nanotubes: molecular dynamics simulations and analytical thermal modelling, Physical Review B 74(12) (2006) 125403.
[37] D. Estrada, E. Pop, Imaging dissipation and hot spots in carbon nanotube network transistors, Applied Physics Letters 98(7) (2011) 073102.
[38] S.L. Zhang, A. Hao, N. Nguyen, A. Oluwalowo, Z. Liu, Y. Dessureault, J.G. Park, R. Liang, Carbon nanotube/carbon composite fiber with improved strength and electrical conductivity via interface engineering, Carbon 144 (2019) 628-638.
[39] S.L. Zhang, N. Nguyen, B. Leonhardt, C. Jolowsky, A. Hao, J.G. Park, R. Liang, Carbon-nanotube-based electrical conductors: fabrication, optimization, and applications. Advanced Electronic Materials 5(6) (2019) 1800811.
[40] E. Herve, Thermal and thermoelastic behaviour of multiply coated inclusion-reinforced composites, International Journal of Solids and Structures 39 (2002) 1041–1058.
[41] Y. Fang, L.Y. Li, S.H. Jang, Calculation of electrical conductivity of self-sensing carbon nanotube composites. Composites B 199 (2020) 108314.
[42] Y. Fang, L.Y. Li, S.H. Jang, Piezoresistive modelling of CNTs reinforced composites under mechanical loadings, Compos. Sci. and Tech. 208 (2021) 108757.
[43] K. Tsuchiya, A. Sakai, T. Nagaoka, K. Uchida, T. Furukawa, H. Yajima, High electrical performance of carbon nanotubes/rubber composites with low percolation threshold prepared with a rotation–revolution mixing technique, Composites Science and Technology 71(8) (2011) 1098-1104.
[44] M.H. Al-Saleh, Clay/carbon nanotube hybrid mixture to reduce the electrical percolation threshold of polymer nanocomposites, Composites Science and Technology 149 (2017) 34-40.
[45] D. Wu, M. Wei, R. Li, T. Xiao, S. Gong, Z. Xiao, Z. Zhu, Z. Li, A percolation network model to predict the electrical property of flexible CNT/PDMS composite films fabricated by spin coating technique, Composites Part B: Engineering 174 (2019) 107034.
[46] W. Xu, Y. Zhang, J. Jiang, Z. Liu, Y. Jiao, Thermal conductivity and elastic modulus of 3D porous/fractured media considering percolation, International Journal of Engineering Science 161 (2021) 103456.
[47] A. Agrawal, A. Satapathy, Development of a heat conduction model and investigation on thermal conductivity enhancement of AlN/Epoxy composites, Procedia Engineering 51 (2013) 573-578.
[48] E. Lizundia, A. Oleaga, A. Salazar, J.R. Sarasua, Nano- and microstructural effects on thermal properties of poly (l-lactide)/multi-wall carbon nanotube composites, Polymer 53(12) (2012) 2412-2421.
[49] Z. Han, A. Fina, Thermal conductivity of carbon nanotubes and their polymer nanocomposites: A review, Progress in Polymer Science 36(7) (2011) 914-944.
[50] W.-T. Hong, N.-H. Tai, Investigations on the thermal conductivity of composites reinforced with carbon nanotubes, Diamond and Related Materials 17(7–10) (2008) 1577-1581.
[51] A. Oluwalowo, N. Nguyen, S.L. Zhang, J.G. Park, R. Liang, Electrical and thermal conductivity improvement of carbon nanotube and silver composites, Carbon 146 (2019) 224-231.

[52] N. Nguyen, S.L. Zhang, A. Oluwalowo, J.G. Park, K. Yao, R. Liang, High-performance and lightweight thermal management devices by 3D printing and assembly of continuous carbon nanotube sheets, ACS Applied Materials & Interfaces 10(32) (2018) 27171-27177.
[53] S.L. Zhang, Y. Ma, L. Suresh, A. Hao, M. Bick, S.C. Tan, J. Chen, Carbon nanotube reinforced strong carbon matrix composites, ACS Nano 14(8) (2020) 9282-9319.

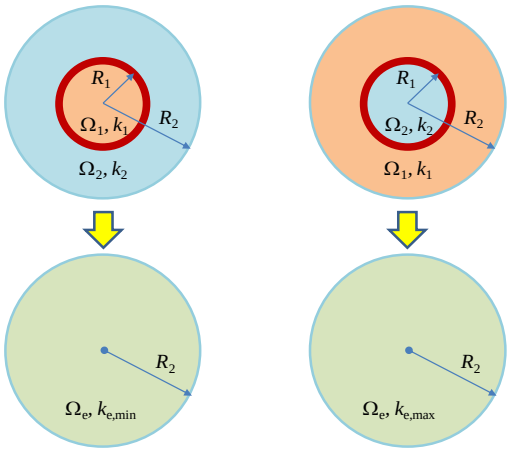

(a) (b)

Fig.1 Spherical model. (a) Two-phase composite where inclusions are embedded in the medium. (b) Two-phase composite where the medium is enclosed by inclusions.

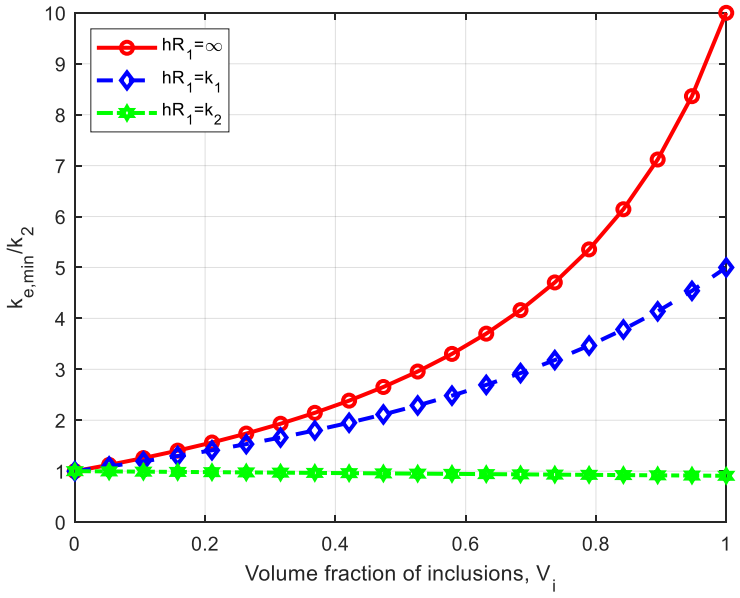

Fig.2 The lower-bound ETC versus volume fraction of inclusions at different interfacial thermal resistances (k_1/k_2=10).

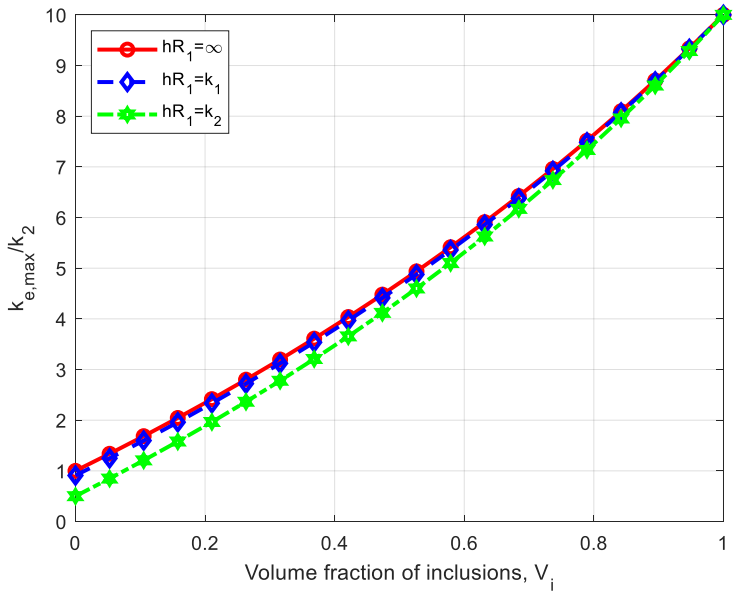

Fig.3 The upper-bound ETC versus volume fraction of inclusions at different interfacial thermal resistances (k_1/k_2=10).

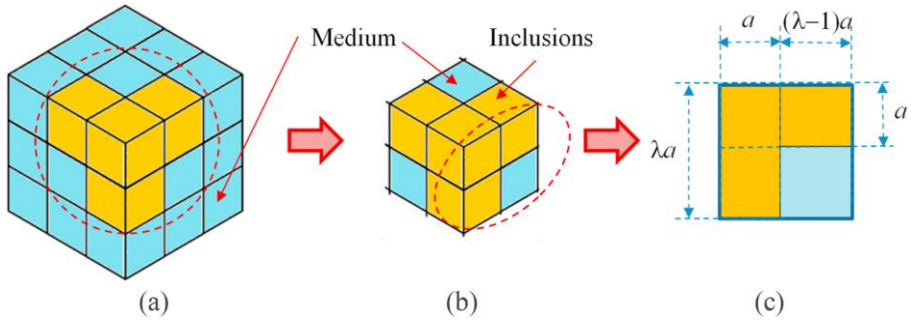

Fig.4. Schematic of fibre-reinforced composite material (blue and yellow represent medium and inclusions). (a) A unit volume cube of RVE of composite. (b) Subdomain involving inclusions. (c) Side view and dimensions of sub-domain [41].

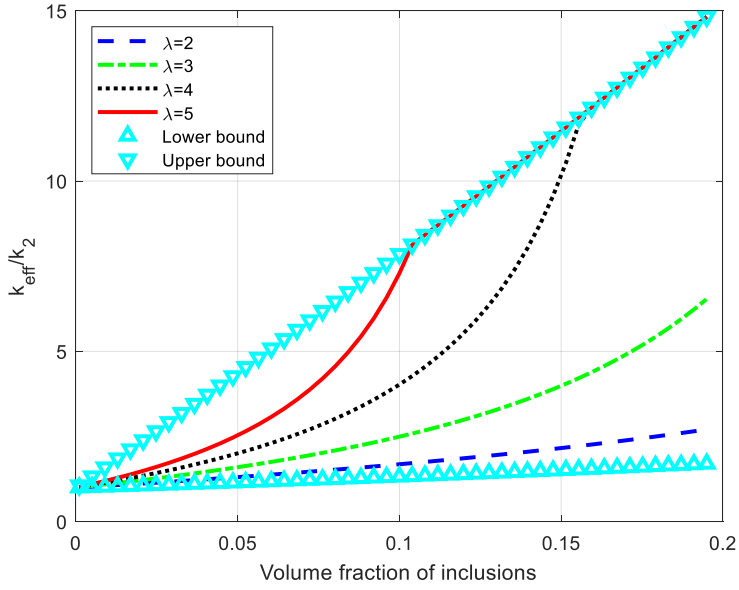

(a)

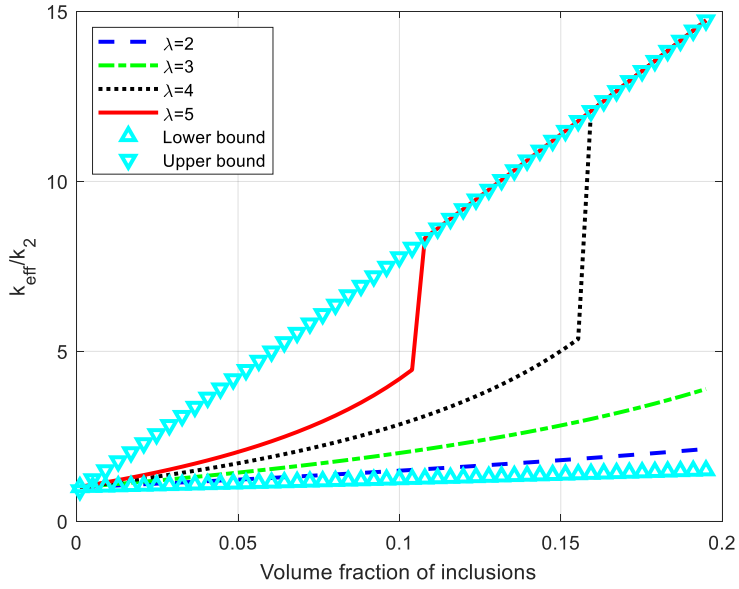

(b)

Fig.5 ETC versus volume fraction of inclusions for different aspect ratios of inclusions (k_1/k_2=100). (a) $hR_1 = \infty$ and (b) $hR_1 = \sqrt{k_1 k_2}$.

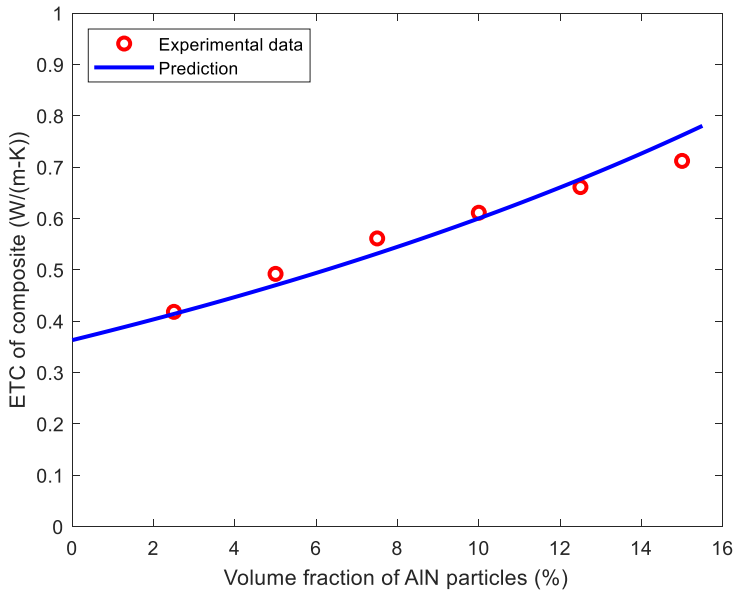

Fig.6 Comparison between analytically predicted and experimentally measured ETCs of AlN-reinforced epoxy composites (k_2=0.363 W/(m·K), λ=2.65, $hR_1=5k_2$).

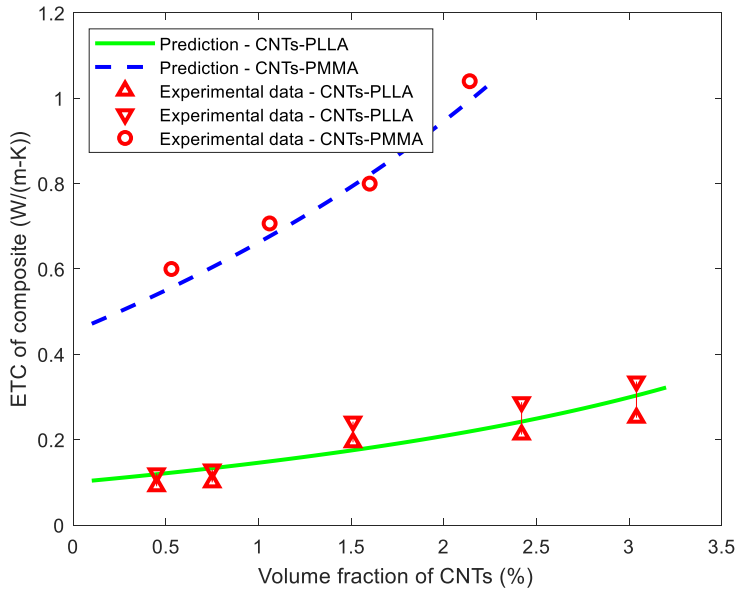

Fig.7 Comparison between analytically predicted and experimentally measured ETCs of CNTs-reinforced polymer composites (k_2=0.10 W/(m·K), λ=8, $hR_1=5k_2$ for PLLA and k_2=0.45 W/(m·K), λ=8, $hR_1=5k_2$ for PMMA).